THE JOURNAL OF PHYSICAL CHEMISTRY A
A JOURNAL OF THE AMERICAN CHEMICAL SOCIETY

pubs.acs.org/JPCA

Article

Quantitative Identification of Nonpolar Perfluoroalkyl Substances by Mass Spectrometry

Jacob Stamm, Lindsey DeJesus, A. Daniel Jones, and Marcos Dantus*

Cite This: J. Phys. Chem. A 2022, 126, 8851−8858

Read Online

ACCESS | Metrics & More | Article Recommendations | Supporting Information

ABSTRACT: Identifying and quantifying mixtures of compounds with very similar fragmentation patterns in their mass spectra presents a unique and challenging problem. In particular, the mass spectra of most per- and poly-fluoroalkyl substances (PFAS) lack a molecular ion. This complicates their identification, especially when using the absence of chromatographic separation. Here, we focus on linear, nonpolar, short-chain PFAS, which have received less attention than amphipathic PFAS despite their longer environmental lifetimes and greater global warming potentials. We identify and quantify *n*-C_5F_{12} and *n*-C_6F_{14} in binary mixtures by analyzing small changes in abundances of the main fragment ions following femtosecond tunnel laser ionization, without the need of chromatographic separation. Time-resolved femtosecond ionization mass spectrometry reveals that the metastable cation of both compounds undergoes predissociation within 1−2 ps of ion formation, with yields of $C_3F_7^+$ showing evidence of coherent vibrational dynamics. These coherent oscillations are compared to low-level ion-state calculations and supported the idea that the oscillations in the $C_3F_7^+$ ion yield are due to vibrations in the $C_5F_{12}^{+\bullet}$ and $C_6F_{14}^{+\bullet}$ radical cations and are associated with the predissociation dynamics of the metastable molecular ion. Surprisingly, we find that the fragment ions used for quantifying the mixtures have similar fragmentation dynamics. Conversely, the odd-electron $C_2F_4^{+\bullet}$ fragment shows different time dependence between the two compounds, yet has negligible difference in the relative ion yield between the two compounds. Our findings indicate that femtosecond laser ionization may be a useful tool for identifying and quantifying mixtures of PFAS without the need of chromatography or high-resolution mass spectrometry.

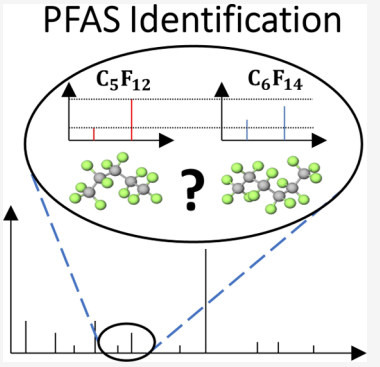

1. INTRODUCTION

Due to the strength of the carbon−fluorine bond, per- and poly-fluoroalkyl substances (PFAS) have been used in great quantities as fire-suppressants, surfactants, stain repellants, and non-reactive coatings.[1] PFAS comprise a group of thousands of compounds that undergo little or no degradation in the environment, hence the "forever chemicals" designation, and have been found in trace quantities in most animals, including humans.[2,3] The widespread use of these compounds and their longevity lead to bioaccumulation, presenting a hazard to humans and entire ecosystems. Indeed, several studies show connections between PFAS bioaccumulation, cancer, and decreased fertility.[4,5] The long-term environmental impact of these materials arises from their global warming potential, which is nearly 10,000 greater than that of CO_2 (time horizon 100 years).[6] Identification and characterization of these compounds are quite important as they allow us to track their spread and possibly identify sources of PFAS contamination. Most research on identification of PFAS focuses on molecules with a polar headgroup and a nonpolar C−F tail. These compounds are chosen for study due to their solubility in water, which also grants them properties allowing for transport in environmental media and uptake into biota.

Identifying the >10,000 different man-made PFAS that are estimated to be present in the environment, in our food, and in our bodies, using standard electron-ionization mass spectrometry (EI-MS) is extremely challenging because the molecular ion is absent. Among the characteristics that make PFAS identification difficult by EI-MS are the strength of C−F bonds compared to C−C bonds and the propensity of these compounds to undergo dissociative electron attachment, which explains why in most cases the molecular ion is absent.[7] Among the established methods aimed at addressing these challenges include liquid chromatography (LC) coupled with either tandem mass spectrometry (LC−MS/MS),[8] high-performance LC combined with inductively coupled plasma mass spectrometry (HPLC-ICP-MS/MS);[9] and LC/ion mobility-quadrupole time-of-flight (TOF) MS (LC/IM-QTOF-MS).[10] In particular, high-resolution MS (HRMS) has achieved non-targeted identification of PFAS, without the need for authentic chemical standard synthesis for confirmation.[11] Current EPA approved methods for quantification of

Received: July 29, 2022
Revised: October 7, 2022
Published: November 16, 2022

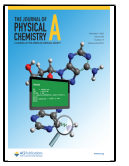

PFAS are limited to a subset of available analytical isotopic standards, all of which are polar.[12−16] Here, we present a method for differentiation between linear, nonpolar, short-chain PFAS molecules using TOF mass spectrometry (MS) without the need for LC, MS/MS, IM-QTOF, or HRMS.

n-C_xF_y compounds undergo fast, nonstatistical dissociation, which further complicates their identification. For example, C_2F_6 and C_3F_8 were found to dissociate promptly upon electron ionization, and neither the positive or negative molecular ions were observed.[17] This conclusion was reached by noting that statistical theory failed to reproduce the observed ion yields involving C−C or C−F bond cleavage. In other words, if the excess energy was distributed throughout the molecule prior to dissociation, little or no C−F bond cleavage would be observed. It has been estimated that upon ionization, C_2F_6 produces CF_3^+ + CF_3 on a timescale comparable with a single vibration.[18] The fast dissociation can be explained by the ionic ground state being crossed by a repulsive state that correlates with products that lie below the ionization potential (IP). In this case, predissociation takes place on a timescale that depends on the curve crossing process. This concept is illustrated in Figure 1 for stable and

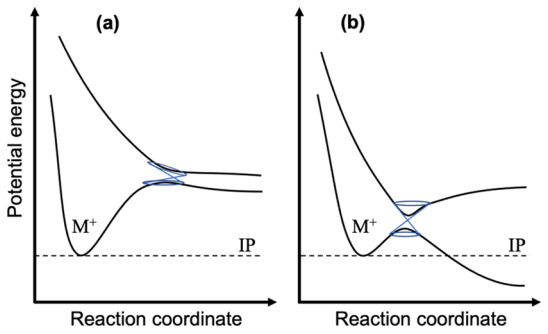

Figure 1. Schematic representation of cuts along the potential energy surfaces illustrating the crossing of the ground ionic state (M^+) with a repulsive ionic state, giving rise to a conical intersection indicated in blue. When the dissociation energy of the repulsive state is higher than the IP, the ground ionic state M^+ is stable (a). When the dissociation energy of the repulsive state is lower than the IP, predissociation via tunneling is possible, and M^+ is metastable (b).

metastable molecular ions. As shown in Figure 1a, the ground ionic state, even if crossed by another state, correlates with reactions having a dissociation energy that is above the IP. As shown in Figure 1b, the ionic ground state is crossed by a repulsive potential correlating with a dissociation energy that is below the IP. In both cases, the crossing between the multidimensional surfaces is illustrated by a conical intersection. The lifetime of the metastable molecular ion, as shown in Figure 1b, depends on the height of the barrier and its vibrational energy.

The appearance potentials for *n*-C_3F_8 and *n*-C_4F_{10}, obtained via threshold photoelectron−photoion coincidence spectroscopy using vacuum-ultraviolet radiation, provide valuable information regarding the dissociative ionization of the two compounds studied here.[19] These values should be compared with the thermodynamic dissociation energies for each of the reactions. For *n*-C_4F_{10}, all the reactions have a dissociation energy that is below the appearance energy. This explains why the molecular ion of most PFAS is metastable, as shown in Figure 1b and not observed in mass spectra. The energetics, as provided in Table 1, allow us to appreciate the difference

Table 1. Dissociation Channels and Appearance Energies for *n*-C_3F_8 and *n*-C_4F_{10}

parent molecule	dissociation channel	dissociation energy (eV)[19]	appearance energy (eV)
n-C_3F_8	→ CF_3^+ + C_2F_5	12.96	13.22 ± 0.02[40]
	→ $C_2F_5^+$ + CF_3	13.71	13.32 ± 0.02[40]
	→ $C_2F_4^+$ + CF_4	12.07	13.5 ± 0.1[41]
	→ $C_3F_7^+$ + F	16.05	15.44 ± 0.02[40]
n-C_4F_{10}	→ CF_3^+ + C_3F_7	12.34	12.6 ± 0.4[19]
	→ $C_3F_6^+$ + CF_4	11.16	12.6 ± 0.1[19]
	→ $C_2F_4^+$ + C_2F_6	11.26	12.6 ± 0.4[19]
	→ $C_2F_5^+$ + $C_2F_5^+$	12.64	13.0 ± 0.4[19]
	→ $C_4F_9^+$ + F	14.95	15.7 ± 0.3[19]

between breaking a C−C bond to produce CF_3^+ compared to breaking a C−F bond to produce $C_4F_9^+$. Unfortunately, no such data are available for *n*-C_5F_{12} and *n*-C_6F_{14}.

Our study focuses on dodecafluoropentane, *n*-C_5F_{12} PFC-4-1-12, and tetradecafluorohexane, *n*-C_6F_{14} PFC-5-1-14, which are used as refrigerants, precision cleaning solvents, and fire extinguishants. C_6F_{14} is also used in medicine as an imaging agent for echocardiograms, improving pulmonary compliance, and treating the lungs of burn victims. These compounds, in addition to being directly synthesized, can result from the electrochemical degradation of PFAS compounds.[20] Thermal treatments may also convert various PFAS chemicals to volatile perfluorocarbons, presenting significant challenges for the development of lower-energy thermal treatments for PFAS destruction. Unfortunately, common mass spectrum libraries have given less than desirable spectral matches for some volatile PFAS pyrolysis products.[21] Improving environmental mapping of these highly volatile and long-lived PFAS compounds requires strategies for their identification and quantification. Here, we address the challenge of identifying and quantifying mixtures of nonpolar PFAS molecules using MS.

2. METHODS

For strong field ionization (SFI) MS measurements, we employed a 1 kHz repetition rate regeneratively amplified titanium−sapphire laser (Legend, Coherent), generating 36 fs pulses full width at half-maximum at an 800 nm central wavelength. The pulses are compressed to their transform limit by a programmable pulse shaper (MIIPS-HD, IPG Photonics) and the multiphoton intrapulse interference phase scan compression method.[22,23] These pulses are focused onto a diffuse stream of gas molecules in a Wiley−McLaren TOF mass spectrometer detecting positively charged fragments. The estimated resolution of the home built TOF is 500. When focused, each pulse had an intensity up to 8×10^{14} W/cm^2. This and subsequent intensities have been determined using Ar^{2+}/Ar^+ ratios as a function of laser intensity.[24] Laser power fluctuations were <2% throughout the data collection process. A sample of each pure compound is introduced as vapor into the mass spectrometer without chromatographic separation, and the relative areas for all peaks are evaluated.

The molecular ion of both compounds was not observed and thus could not be used for identification or quantification. We have access to the pure samples to acquire reference spectra, implying that we performed a targeted identification. The relative peak areas for each pure compound allow for calibration for the quantification process. To quantify the two

https://doi.org/10.1021/acs.jpca.2c05373
J. Phys. Chem. A 2022, 126, 8851−8858

PFAS molecules, eight mixtures containing liquid C_5F_{12} and C_6F_{14} with varying molar fractions were made by a third party and subjected to measurements. The experiments on the pure compounds and the mixtures were performed using three sets of laser conditions: 8×10^{14} W/cm^2 linearly polarized light, 4×10^{14} W/cm^2 circularly polarized light, and 5×10^{14} W/cm^2 linearly polarized light. In the case of linearly polarized pulses, the laser's electric field was aligned along the TOF axis. These measurements were carried out with a single pump pulse at the listed laser intensities. Under these conditions, molecules may undergo tunnel ionization, a process that is very sensitive to molecular structure and polarizability.[25]

For time-resolved measurements, the pulse was split into a strong pump (5×10^{14} W/cm^2) and a weak probe (7×10^{13} W/cm^2) using a beam splitter. The delay between these two pulses was controlled by a programmable optical delay line, and the intensity of the probe was adjusted until it no longer generated ions on its own. We use an approach we call "disruptive probing," which allows us to simultaneously keep track of tens of reaction pathways.[26] Briefly, the pump pulse causes SFI of the molecules under study. Molecules become ionized and acquire 10−30 eV of additional internal energy through electron recollision.[27] The ensuing chemical reactions are tracked by the weak probe pulse, which can disrupt or enhance the formation of a given product ion. Therefore, the signal as a function of time delay may show a depletion or an enhancement in the product ion yield, compared to the yield observed at negative delay times. The recovery time following disruption provides us with a timescale for the formation of a particular product.

3. RESULTS AND DISCUSSION

3.1. PFAS Identification by SFI. Upon interaction with intense femtosecond pulses, these compounds undergo similar fragmentation and yield negligible parent molecular ions; hence, they have nearly identical mass spectra, as shown in Figure 2. The fragmentation mechanisms of PFAS in MS have received limited attention. Studies on polar PFAS following fast-atom bombardment identified two series of peaks characterized by a loss of CF_2 (m/z 50) that follow the formulas $C_nF_{2n+1}^+$ (m/z 69, 119, and 169) and $C_nF_{2n}^{+\bullet}$ (m/z 50, 100, and 150).[28,29] The latter series of odd-electron cations possibly occurs via intramolecular rearrangement involving the migration of a fluorine anion to the neutral fragment.

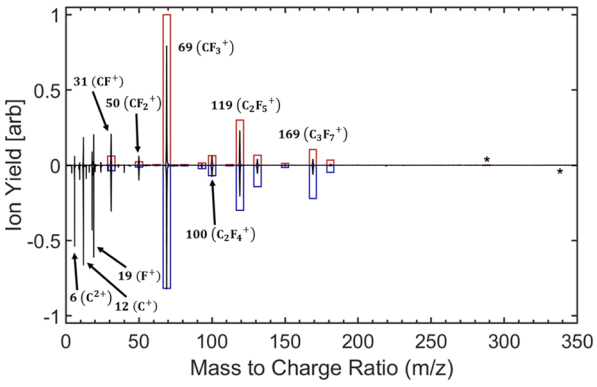

Figure 2. Femtosecond laser ionization mass spectrum of C_5F_{12} (top) and C_6F_{14} (bottom) along with the NIST mass spectra which use electron ionization (red and blue boxes). The expected location of the molecular ions for both compounds has been labeled with an asterisk, and several abundant peaks in the mass spectrum have been labeled. Both the femtosecond and NIST spectra have been normalized to the sum of the ions shared by both MS. Nitrogen and oxygen peaks from a small amount of air have been removed for clarity.

In our spectra, when using higher laser intensities, we observe one additional series with formula $C_nF_{2n-1}^+$ (m/z 31, 81, and 131). The fragmentation of such PFAS upon electron ionization was said to be remote charge site fragmentation.[28,29] For the linear perfluoroalkanes considered here, the fragmentation is like that of saturated *n*-alkanes, for which the molecular ion is very small or not observed. For alkanes, fragmentation leads to the ion series with formulas ($C_nH_{2n+1}^+$, $C_nH_{2n}^+$, and $C_nH_{2n-1}^+$) with peaks separated by m/z 14, corresponding to the loss of CH_2 fragments. The dominant mechanism of linear alkane fragmentation is σ-cleavage involving secondary carbons, followed by σ cleavage of CH_2 moieties.[30] Based on projects by our group and others aimed at the identification and quantification of isomeric mixtures using femtosecond SFI MS,[31−34] we explore if a similar approach can be used to identify and quantify mixtures of PFAS. Quantitative mass spectrometric identification without chromatographic separation of isomeric mixtures by femtosecond laser pulse ionization was pioneered by Dela Cruz et al.[31,32] Multidimensional MS was accomplished by using differently shaped laser pulses to improve the identification of warfare agents and the analysis of mixtures of isomers.[35,36] Advantages of SFI-MS include their speed, sensitivity, and minimal analyte usage. Multivariate linear regression based on the spectrum of each isomer carried separately following SFI was used to quantify mixtures of allene and propyne, C_3H_4 isomers.[37] The chirped pulses were used to analyze ternary mixtures of *ortho*-, *meta*-, and *para*-fluorotoluene.[33] More recently, binary and ternary mixtures of *ortho*, *meta*, and *para*-nitrotoluene were analyzed by comparing the time-dependence of the parent molecular ion following 1300 nm pump and 650 nm probe pulses.[34]

The key for identifying between the two PFAS compounds is to capitalize on small differences in certain ion yields between the two compounds. To do this, the 16 largest peaks in the mass spectrum are chosen to represent the total ion yield. The 16 peaks are integrated, and their areas are summed. The entire MS is then divided by this sum. The normalization is carried out to minimize overall ion yield differences caused by differences in detector sensitivity, vapor pressure, polarizability, and IP between the two samples. Table 2 shows the relative areas of the 16 highest-yield ions for C_5F_{12} and C_6F_{14}.

We find that the small, combined differences in peak areas, as shown in Table 1, allows for the differentiation between the two PFAS molecules. Once the normalized areas representing the key ion yields for C_5F_{12} and C_6F_{14} are rescaled such that the yield of a particular ion from C_5F_{12} is 1, and the yield of that same ion from C_6F_{14} is 0, the combination of some of the peak areas is mapped onto a scale of the molar fraction. The process of rescaling the normalized peak areas to 0 and 1 is given by the following transformation

$$Y_i \rightarrow \frac{Y_i - Y_{C_6F_{14}}}{Y_{C_5F_{12}} - Y_{C_6F_{14}}} \quad (1)$$

where Y_i is the quantification parameter $(A_{119} + A_{181}) - (A_6 + A_{169})$ for some mixture i and $Y_{C_5F_{12}}$ and $Y_{C_6F_{14}}$ are the quantification parameters for pure C_5F_{12} and pure C_6F_{14}, respectively. Note that substituting $Y_{C_5F_{12}}$ into this equation for

https://doi.org/10.1021/acs.jpca.2c05373
J. Phys. Chem. A 2022, 126, 8851−8858

Table 2. Relative Peak Areas of 16 of the Largest Peaks in the Mass Spectra, Normalized to the Sum of the Areas of All Listed Peaks for Each Pure Compound[a]

fragment ion (m/z)	C_5F_{12}	C_6F_{14}	fragment ion (m/z)	C_5F_{12}	C_6F_{14}
C^{2+} (6)	0.009	0.016	$C_2F_3^+$ (81)	0.004	0.004
C^+ (12)	0.033	0.047	$C_3F_3^+$ (93)	0.009	0.013
F^+ (19)	0.045	0.050	$C_2F_4^+$ (100)	0.052	0.051
C_2^+ (24)	0.020	0.022	$C_2F_5^+$ (119)	0.136	0.121
CF^+ (31)	0.108	0.108	$C_3F_5^+$ (131)	0.038	0.047
CF_2^+ (50)	0.046	0.044	$C_3F_6^+$ (150)	0.004	0.005
CF_3^+ (69)	0.457	0.415	$C_3F_7^+$ (169)	0.029	0.049
$C_3F_2^+$ (74)	0.003	0.004	$C_4F_7^+$ (181)	0.007	0.005

[a]These data were taken with linearly polarized light with 8×10^{14} W/cm^2 intensity.

Y_i yields 1 and substituting $Y_{C_6F_{14}}$ for Y_i yields 0. This transformation then maps the mixtures onto a molar fraction of C_5F_{12}, with the remaining fraction consisting of the C_6F_{14}. This not only allows for the identification of C_5F_{12} and C_6F_{14} molecules but also the quantification of their respective molar fractions in a mixture. The parameter used to determine the molar fraction of each of the two compounds is $(A_{119} + A_{181}) - (A_6 + A_{169})$, where A_n is the relative area of the peak at $m/z = n$ and the areas have been normalized to the sum of the 16 largest peak areas. These ions were chosen to represent the difference because they are the two ions with the largest relative difference in yield that favor C_5F_{12} (A_{119} and A_{181}) and the two ions with the largest relative difference in yield that favor C_6F_{14} (A_6 and A_{169}). Using this parameter and rescaling, we were able to map the data from the mixtures onto a molar fraction of C_5F_{12}. Because the mixtures were prepared from the liquid samples and only the vapor of the mixtures entered the mass spectrometer as an effusive beam for analysis, we used Raoult's law to convert the liquid C_5F_{12} molar fractions into vapor C_5F_{12} molar fractions. Figure 3 shows our measured C_5F_{12} molar fraction versus the actual C_5F_{12} molar fraction, which was revealed to us after the experiment was complete, again, with the remaining component being the C_6F_{14}.

From Figure 3, we may conclude that despite the small differences in peak areas, it is possible to distinguish C_5F_{12} and C_6F_{14} and even quantify their relative abundance in a binary mixture. In the Supporting Information, we show successful quantitative analysis of the mixtures using different ions for the quantification parameter (Figures S1−S4). Furthermore, we show results based on a single mass spectrum (Figure S5), which can be reliably obtained in less than 1 s depending on the laser repetition rate. Since changes in laser intensity will alter the relative ion yields, we also report in the Supporting Information several mass spectra at different laser intensities (Figures S6−S14). We have plans to expand this work to branched and cyclic PFAS compounds and to increase the complexity of the mixtures to three or more components. Only then, will we be able to determine whether this approach has a practical value, especially for analysis of mixtures using LC-MS.

3.2. Reaction Dynamics of PFAS Following SFI. To elucidate the reasons for the differences in the ion yields of these two PFAS molecules, both molecules were analyzed using femtosecond time-resolved MS and disruptive probing.[26,38] Differences in ion yield timescales may be used to understand why one molecule will generate more of a particular fragment. The yields of the same ions in Table 1 were tracked as a function of pump−probe delay and are shown in Figure 4.

Figure 4 shows the time-resolved ion yields for the 16 highest yield ions from both C_5F_{12} (red) and C_6F_{14} (blue). We observe that each of the ions has a feature at zero delay that corresponds to the sum of the pump and probe pulses, also known as the "coherent spike." This feature has a Gaussian shape with a duration proportional to that of the laser pulses. The interpretation and fitting of disruptive-probing transients have been described elsewhere.[26] It is important to remember that only the pump laser is intense enough to cause ionization. For this reason, the data are normalized such that the negative time ion yield equals one. Because the probe pulse is weak, it can only deplete or enhance the ion yield with respect to its value for negative time delay when the precursor ion is far from equilibrium. The recovery time following depletion is related to the reaction time to form the product.

We explain the three different time-resolved behaviors observed for the PFAS as follows. Following the zero-delay feature, most ions (m/z 69, 119, 131, 150, 169, and 181) exhibit a fast depletion followed by a slow recovery (1−2 ps)

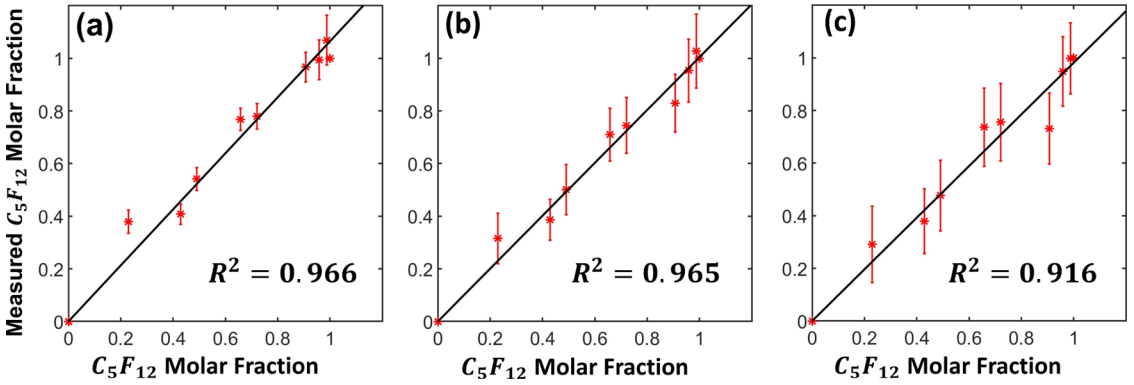

Figure 3. Measured C_5F_{12} molar fraction vs actual C_5F_{12} molar fraction. The remaining fraction of the binary mixture is the C_6F_{14}. Quantified mixtures are shown for (a) linear polarization with 8×10^{14} W/cm^2 intensity, (b) linear polarization with 5×10^{14} W/cm^2 intensity, and (c) circular polarization with 4×10^{14} W/cm^2 intensity. Data points for each of the two pure compounds and eight mixtures are shown as red stars, and the linear trendline is shown as a black line. R^2 values are shown to compare each of the laser conditions. Error bars show ±1 standard deviation in the measured molar fraction. The error bars are found by taking the standard deviation of peak areas from 100 spectra, each of which is the average of ∼2500 laser shots. These standard deviations are transformed into errors in the molar fraction using propagation of error.

https://doi.org/10.1021/acs.jpca.2c05373
J. Phys. Chem. A 2022, 126, 8851−8858

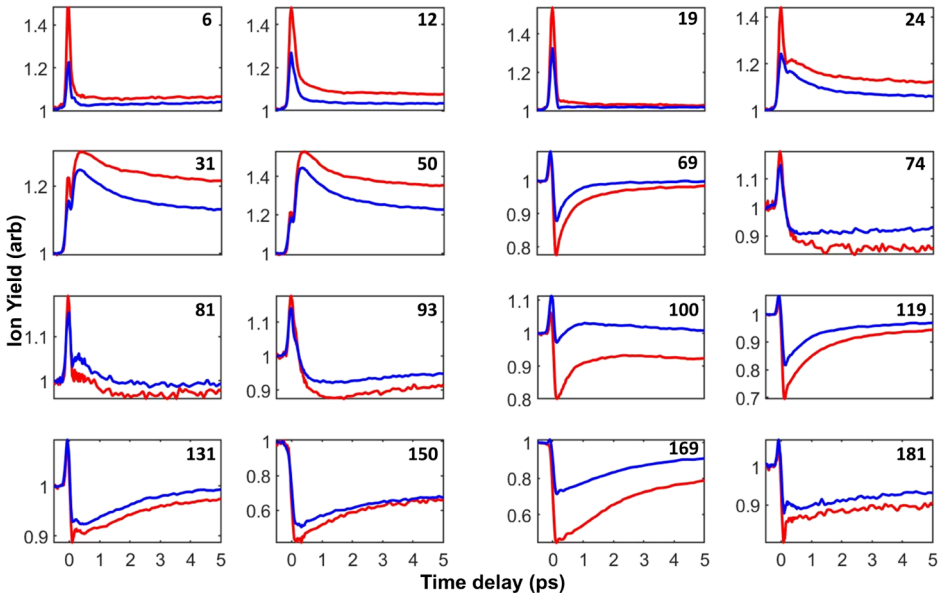

Figure 4. Ion yields as a function of pump−probe delay for C_5F_{12} (red) and C_6F_{14} (blue). Ion yields are normalized, so negative time delays have ion yield of unity. The mass-to-charge ratio is indicated in black in the upper right-hand corner of each panel.

rise. Ions (m/z 6, 12, 19, 24, 31, and 50) exhibit fast enhancement in yields, indicating that the probe enhances their yields while the precursor ion is far from equilibrium. Note that these enhanced-yield ions are lower in mass, and their yields increase as the larger ions are fragmented by the probe pulse. Atomic ions with m/z 6, 12, and 19 are primarily observed while both pulses are overlapped and m/z 31 (CF^+) and 50 (CF_2^+) exhibit a ∼200 fs rise time. Ions with m/z 74, 81, and 93 show a slow depletion followed by an even slower rise. We note that the m/z 100 ($C_2F_4^+$) ion yield shows depletion for C_5F_{12} but enhancement for C_6F_{14} (blue). We address this difference later. Interestingly, the ions used for identifying and quantifying mixtures of these two compounds (m/z 6, 119, 169, and 181) have similar ultrafast reaction dynamics (Figure 4). To be certain that the time-resolved differences are similar, in the Supporting Information we show some of these key transients manipulated to overlap their depletion regions (Figures S15−S18). This manipulation aids the reader in comparing timescales. The similarity of the reaction dynamics observed in the two PFAS compounds implies that the small difference in yield of these ions is possibly due to the odd and even number of carbons and slight differences in the polarizability between these molecules.

We analyze these ion yield curves by looking at correlations.[8] We calculated the Pearson correlation coefficient for the time-dependent ion yield curves, where the correlation between a pair of curves is found by

$$r_{ij} = \frac{N\left(\sum_{k=1}^{N} Y_{ik}Y_{jk}\right) - \left(\sum_{k=1}^{N} Y_{ik}\right)\left(\sum_{k=1}^{N} Y_{jk}\right)}{\sqrt{\left[N\sum_{k=1}^{N} {Y_{ik}}^2 - \left(\sum_{k=1}^{N} Y_{ik}\right)^2\right]\left[N\sum_{k=1}^{N} {Y_{jk}}^2 - \left(\sum_{k=1}^{N} Y_{jk}\right)^2\right]}} \quad (2)$$

where N is the number of pump−probe scans and Y_{ik} and Y_{jk} are the yields of ions i and j at pump−probe time delay k. These coefficients are computed for each pair of ions and summarized in a correlation diagram, as shown in Figure 5.

From Figure 5, we see that fragment ion $C_2F_4^+$ (m/z 100), not used for identification purposes, has a different time-dependent ion yield despite having similar yield under a single laser pulse. Such a difference in correlation for m/z 100 could be explained by reaction channels that are present in one molecule but absent in the other, potentially due to an odd/even effect with the number of carbons. We explain this hypothesis later. The difference in the reaction dynamics of this fragments dynamics is shown more clearly in the Supporting Information (Figure S16).

In addition to the correlation diagrams, further analysis of the time-resolved data in Figure 4 shows small coherent oscillations in $C_3F_7^+$ (m/z 169). These oscillations were isolated by subtracting the slower picosecond dynamics. Figure 6 shows the oscillations in this fragment from C_5F_{12} (red) and C_6F_{12} (blue). Fitting the oscillations to a sinusoidal function yielded a period of 265 ± 5 fs for $C_3F_7^+$ from C_5F_{12} and 276 ± 11 fs for $C_3F_7^+$ from C_6F_{14}. The oscillations are presumed to be in normal modes in the respective parent ion, excited by the pump pulse following ionization. This hypothesis is analyzed further below. The oscillations in the yield decayed due to dephasing with a time constant of 565 ± 110 fs for $C_3F_7^+$ from C_5F_{12} and 438 ± 130 fs for $C_3F_7^+$ from C_6F_{14}.

To elucidate the cause of these oscillations in $C_3F_7^+$ yield as a function of pump−probe delay, we ran low-level density functional theory calculations on the $C_5F_{12}^+$ and $C_6F_{14}^+$ radical cations using the 6-31G* basis set in the Spartan program.[39] The results of these ion state calculations yielded a Raman spectrum for each of these molecular ions, from which we found low-frequency modes with energies in the range 0−300 cm^{-1}. It should be noted that despite being metastable, the molecular ion can still undergo vibrations before dissociation. Given the complexities of carrying out higher level calculations on the radical cations of perfluorinated compounds, we are not able to provide accurate mode assignments and frequencies. Thus, we are left to assume these low-frequency vibrations in the ion state in the process of predissociation to the yield of $C_3F_7^+$.

https://doi.org/10.1021/acs.jpca.2c05373
J. Phys. Chem. A 2022, 126, 8851−8858

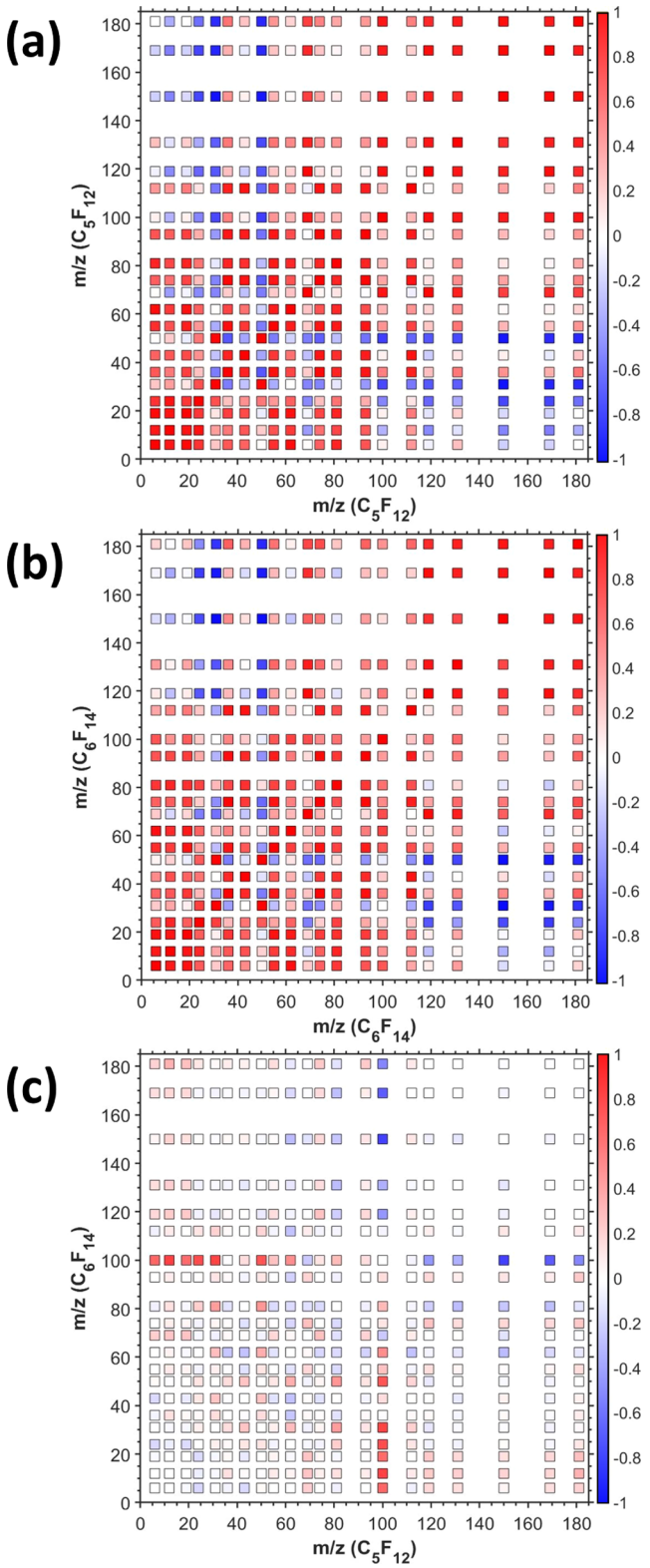

Figure 5. Correlation diagrams for (a) ions from C_5F_{12} with ions from C_5F_{12}, (b) ions from C_6F_{14} with ions from C_6F_{14}, and (c) difference diagram between correlations (a,b). The color bars indicate the value of the Pearson correlation coefficient for each color. Red is a positive correlation, blue is a negative correlation, and white is no correlation.

While the time-resolved data did not identify the cause of the differences observed in some of the ion yields between C_5F_{12} and C_6F_{14}, it did allow for some insights into the molecular dynamics following ionization by the pump pulse. Namely, reactions occur in a 1−2 ps timescale, with very small evidence of coherent vibrational motion in only one fragment. Furthermore, no relationship between differences in ion yield and differences in reaction timescale was found. Some ions (m/z 6, 119, 169, and 181) exhibited large relative ion yield differences (Table 1) following single pulse ionization, but when the reaction dynamics were probed, no dynamic differences were observed (Figure 4). An expanded comparison that superimposes the time-resolved data for a few ions is included in Supporting Information (Figures S15−S18).

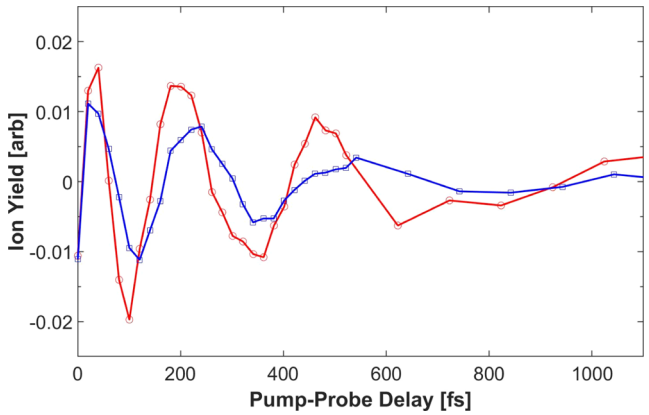

Figure 6. Time-resolved ion yields for $C_3F_7^+$ (m/z 169) from C_5F_{12} (red) and C_6F_{14} (blue), exhibiting coherent oscillations in the yield. These oscillations take place during predissociation of the molecular ion.

Looking at the correlations between the time-dependent yields of all the ions (Figure 5c), the odd-electron ion $C_2F_4^+$ (m/z 100) has different dynamics when being generated from C_5F_{12} versus C_6F_{14} (Figure 4). For C_5F_{12}, the probe depletes the yield of that product, but for C_6F_{14}, the probe enhances the yield. This implies that following the initial pulse, there is a species that can be turned into $C_2F_4^+$ by the probe pulse. The precursor species of this ion are likely $C_3F_7^+$ or $C_3F_5^+$, both of which are produced in greater yield by C_6F_{14}.

4. CONCLUSIONS

In conclusion, we find that femtosecond SFI is capable of identifying and quantifying mixtures of C_5F_{12} and C_6F_{14}. The identification becomes possible because of small differences in the ion yield between the two compounds. This quantification was carried out without chromatographic separation or HRMS. Femtosecond time-resolved measurements revealed very similar reaction dynamics. The reactions occur in a 1−2 ps timescale, a time which is associated with the lifetime of the metastable ground ionic state. The observation of short-lived coherent vibrational dynamics in the m/z $C_3F_7^+$ fragment from both molecules corresponds to vibrations during the predissociation process. When comparing these oscillations to the inverse Fourier transformed Raman spectrum of the low-level calculated ion states, it supported the idea that the oscillations in $C_3F_7^+$ are due to vibrations in the $C_5F_{12}^+$ and $C_6F_{14}^+$ ions. In the future, we plan to expand this work to branched and cyclic PFAS and more complex mixtures to determine whether it is viable for analysis of environmental samples and diagnostics of PFAS remediation processes. As we refine the method, we will seek better R^2 values and reduce data acquisition time from 2.5 to 0.25 s. We hope that

https://doi.org/10.1021/acs.jpca.2c05373
J. Phys. Chem. A 2022, 126, 8851−8858

information about reaction times and dephasing rates will help theory efforts into elucidating molecular fragmentation following electron ionization.

■ ASSOCIATED CONTENT

Supporting Information

The Supporting Information is available free of charge at https://pubs.acs.org/doi/10.1021/acs.jpca.2c05373.

Comparison of other combinations of relative ion yields to quantify the PFAS mixtures, quantification from a single measurement (~2500 laser shots at 1 kHz) with included R^2 parameters, PFAS spectra as a function of laser intensity (no molecular ion seen in any of the listed laser intensities), and time-resolved ion yield curves for several key ions (normalized to further illustrate the similarities of the timescales of formation for several key ions) (PDF)

■ AUTHOR INFORMATION

Corresponding Author

Marcos Dantus − *Department of Chemistry and Department of Physics and Astronomy, Michigan State University, East Lansing, Michigan 48824, United States;* orcid.org/0000-0003-4151-5441; Email: dantus@msu.edu

Authors

Jacob Stamm − *Department of Chemistry, Michigan State University, East Lansing, Michigan 48824, United States*

Lindsey DeJesus − *Department of Chemistry, Michigan State University, East Lansing, Michigan 48824, United States*

A. Daniel Jones − *Department of Biochemistry and Molecular Biology and Center for PFAS Research, Michigan State University, East Lansing, Michigan 48824, United States;* orcid.org/0000-0002-7408-6690

Complete contact information is available at: https://pubs.acs.org/10.1021/acs.jpca.2c05373

Notes

The authors declare no competing financial interest.

■ ACKNOWLEDGMENTS

This material is based upon work supported by the Air Force Office of Scientific Research under award number FA9550-21-1-0428. We thank Bethany Jochim for training and supervising Lindsey DeJesus during data acquisition and Leo Suguimoto Specht for his help in fitting some of the time-resolved data.

■ REFERENCES

(1) Glüge, J.; Scheringer, M.; Cousins, I. T.; DeWitt, J. C.; Goldenman, G.; Herzke, D.; Lohmann, R.; Ng, C. A.; Trier, X.; Wang, Z. An Overview of the Uses of Per- and Polyfluoroalkyl Substances (PFAS). *Environ. Sci.: Processes Impacts* **2020**, *22*, 2345−2373.

(2) Sunderland, E. M.; Hu, X. C.; Dassuncao, C.; Tokranov, A. K.; Wagner, C. C.; Allen, J. G. A Review of the Pathways of Human Exposure to Poly- and Perfluoroalkyl Substances (PFASs) and Present Understanding of Health Effects. *J. Exposure Sci. Environ. Epidemiol.* **2019**, *29*, 131−147.

(3) Rahman, M. F.; Peldszus, S.; Anderson, W. B. Behaviour and Fate of Perfluoroalkyl and Polyfluoroalkyl Substances (PFASs) in Drinking Water Treatment: A Review. *Water Res.* **2014**, *50*, 318−340.

(4) Mottaleb, M. A.; Petriello, M. C.; Morris, A. J. High-Throughput UHPLC-MS/MS Measurement of Per- and Poly-Fluorinated Alkyl Substances in Human Serum. *J. Anal. Toxicol.* **2020**, *44*, 339−347.

(5) Calvert, L.; Green, M. P.; de Iuliis, G. N.; Dun, M. D.; Turner, B. D.; Clarke, B. O.; Eamens, A. L.; Roman, S. D.; Nixon, B. Assessment of the Emerging Threat Posed by Perfluoroalkyl and Polyfluoroalkyl Substances to Male Reproduction in Humans. *Front. Endocrinol.* **2022**, *12*, 799043.

(6) Hodnebrog, Ø.; Etminan, M.; Fuglestvedt, J. S.; Marston, G.; Myhre, G.; Nielsen, C. J.; Shine, K. P.; Wallington, T. J. Global Warming Potentials and Radiative Efficiencies of Halocarbons and Related Compounds: A Comprehensive Review. *Rev. Geophys.* **2013**, *51*, 300−378.

(7) Christophorou, L. G.; Olthoff, J. K. Electron Interactions With C3F8. *J. Phys. Chem. Ref. Data* **1998**, *27*, 889−913.

(8) D'Agostino, L. A.; Mabury, S. A. Identification of Novel Fluorinated Surfactants in Aqueous Film Forming Foams and Commercial Surfactant Concentrates. *Environ. Sci. Technol.* **2014**, *48*, 121−129.

(9) Heuckeroth, S.; Nxumalo, T. N.; Raab, A.; Feldmann, J. Fluorine-Specific Detection Using ICP-MS Helps to Identify PFAS Degradation Products in Nontargeted Analysis. *Anal. Chem.* **2021**, *93*, 6335−6341.

(10) Yukioka, S.; Tanaka, S.; Suzuki, Y.; Fujii, S.; Echigo, S. A New Method to Search for Per- and Polyfluoroalkyl Substances (PFASs) by Linking Fragmentation Flags with Their Molecular Ions by Drift Time Using Ion Mobility Spectrometry. *Chemosphere* **2020**, *239*, 124644.

(11) Liu, Y.; D'Agostino, L. A.; Qu, G.; Jiang, G.; Martin, J. W. High-Resolution Mass Spectrometry (HRMS) Methods for Nontarget Discovery and Characterization of Poly- and per-Fluoroalkyl Substances (PFASs) in Environmental and Human Samples. *TrAC, Trends Anal. Chem.* **2019**, *121*, 115420.

(12) Rosenblum, L.; Wendelken, S.*Method 533: Determination of Per- and Polyfluoroalkyl Substances in Drinking Water by Isotope Dilution Anion Exchange Solid Phase Extraction and Liquid Chromatography/Tandem Mass Spectrometry*; US Environmental Protection Agency; EPA 815-B-19-020, 2019. https://www.epa.gov/sites/default/files/2019-12/documents/method-533-815b19020.pdf (accessed October 4, 2022).

(13) Shoemaker, J.; Tettenhorst, D.*Method 537.1: Determination of Selected Per- and Polyfluorinated Alkyl Substances in Drinking Water by Solid Phase Extraction and Liquid Chromatography/Tandem Mass Spectrometry (LC/MS/MS)*; U.S. Environmental Protection Agency, Office of Research and Development, National Center for Environmental Assessment: Washington, DC, 2018.

(14) Draft Method 1633 Analysis of Per- and Polyfluoroalkyl Substances (PFAS) in Aqueous, Solid, Biosolids, and Tissue Samples by LC-MS/MS. 2021, https://www.epa.gov/system/files/documents/2021-09/method_1633_draft_aug-2021.pdf (accessed October 4, 2022).

(15) METHOD 8327 Per- AND Polyfluoroalkyl Substances (PFAS) by Liquid Chromatography/Tandem Mass Spectrometry (LC/MS/MS). 2021, https://www.epa.gov/system/files/documents/2021-07/8327.pdf (accessed October 4, 2022).

(16) Other Test Method 45 (OTM-45) Measurement of Selected Per- and Polyfluorinated Alkyl Substances from Stationary Sources. 2021, https://www.epa.gov/sites/default/files/2021-01/documents/otm_45_semivolatile_pfas_1-13-21.pdf (accessed October 4, 2022).

(17) Lifshitz, C.; Long, F. A. Some Observations Concerning the Positive Ion Decomposition of C2F6 and C3F8 in the Mass Spectrometer1. *J. Phys. Chem.* **1965**, *69*, 3746−3751.

(18) Inghram, M. G.; Hanson, G. R.; Stockbauer, R. The Fragmentation of C2F6+. *Int. J. Mass Spectrom. Ion Phys.* **1980**, *33*, 253−261.

(19) Jarvis, G. K.; Boyle, K. J.; Mayhew, C. A.; Tuckett, R. P. Threshold Photoelectron−Photoion Coincidence Spectroscopy of Perfluorocarbons. 1. Saturated Perfluorocarbons C2F6, C3F8, and n-C4F10. *J. Phys. Chem. A* **1998**, *102*, 3219−3229.

(20) Duinslaeger, N.; Radjenovic, J. Electrochemical Degradation of Per- and Polyfluoroalkyl Substances (PFAS) Using Low-Cost Graphene Sponge Electrodes. *Water Res.* **2022**, *213*, 118148.

(21) Alinezhad, A.; Challa Sasi, P.; Zhang, P.; Yao, B.; Kubátová, A.; Golovko, S. A.; Golovko, M. Y.; Xiao, F. An Investigation of Thermal Air Degradation and Pyrolysis of Per- and Polyfluoroalkyl Substances and Aqueous Film-Forming Foams in Soil. *ACS ES&T Engg* **2022**, *2*, 198−209.
(22) Xu, B.; Gunn, J. M.; Cruz, J. M. d.; Lozovoy, V. v.; Dantus, M. Quantitative Investigation of the Multiphoton Intrapulse Interference Phase Scan Method for Simultaneous Phase Measurement and Compensation of Femtosecond Laser Pulses. *J. Opt. Soc. Am. B* **2006**, *23*, 750−759.
(23) Coello, Y.; Lozovoy, V. v.; Gunaratne, T. C.; Xu, B.; Borukhovich, I.; Tseng, C.; Weinacht, T.; Dantus, M. Interference without an Interferometer: A Different Approach to Measuring, Compressing, and Shaping Ultrashort Laser Pulses. *J. Opt. Soc. Am. B* **2008**, *25*, A140−A150.
(24) Guo, C.; Li, M.; Nibarger, J. P.; Gibson, G. N. Single and Double Ionization of Diatomic Molecules in Strong Laser Fields. *Phys. Rev. A: At., Mol., Opt. Phys.* **1998**, *58*, R4271−R4274.
(25) Hankin, S. M.; Villeneuve, D. M.; Corkum, P. B.; Rayner, D. M. Intense-Field Laser Ionization Rates in Atoms and Molecules. *Phys. Rev. A: At., Mol., Opt. Phys.* **2001**, *64*, 13405.
(26) Jochim, B.; DeJesus, L.; Dantus, M. Ultrafast Disruptive Probing: Simultaneously Keeping Track of Tens of Reaction Pathways. *Rev. Sci. Instrum.* **2022**, *93*, 033003.
(27) Blaga, C. I.; Catoire, F.; Colosimo, P.; Paulus, G. G.; Muller, H. G.; Agostini, P.; DiMauro, L. F. Strong-Field Photoionization Revisited. *Nat. Phys.* **2009**, *5*, 335−338.
(28) Kuehl, D. W.; Rozynov, B. Chromatographic and Mass Spectral Studies of Perfluorooctanesulfonate and Three Perfluorooctanesulfonamides. *Rapid Commun. Mass Spectrom.* **2003**, *17*, 2364−2369.
(29) Arsenault, G.; Chittim, B.; McAlees, A.; McCrindle, R.; Potter, D.; Tashiro, C.; Yeo, B. Mass Spectral Studies of Native and Mass-Labeled Perfluorooctanesulfonamides. *Rapid Commun. Mass Spectrom.* **2007**, *21*, 929−936.
(30) McLafferty, F.; Tureček, F.*Interpretation of Mass Spectra*, 4th ed.; University Science Books, 1993.
(31) Dela Cruz, J. M.; Lozovoy, V. v.; Dantus, M. Quantitative Mass Spectrometric Identification of Isomers Applying Coherent Laser Control. *J. Phys. Chem. A* **2005**, *109*, 8447−8450.
(32) Dela Cruz, J. M.; Lozovoy, V. v.; Dantus, M. Isomeric Identification by Laser Control Mass Spectrometry. *J. Mass Spectrom.* **2007**, *42*, 178−186.
(33) Schäfer, V.; Weitzel, K.-M. Qualitative and Quantitative Distinction of Ortho-, Meta-, and Para-Fluorotoluene by Means of Chirped Femtosecond Laser Ionization. *Anal. Chem.* **2020**, *92*, 5492−5499.
(34) McPherson, S. L.; Shusterman, J. M.; López Peña, H. A.; Ampadu Boateng, D.; Tibbetts, K. M. Quantitative Analysis of Nitrotoluene Isomer Mixtures Using Femtosecond Time-Resolved Mass Spectrometry. *Anal. Chem.* **2021**, *93*, 11268−11274.
(35) Dantus, M.; Lozovoy, V. v.; Zhu, X.; Gunaratne, T. Multidimensional Molecular Identification by Laser Control Mass Spectrometry. *Proc. SPIE* **2008**, *6954*, 69540D.
(36) Pastirk, I.; Zhu, X.; Lozovoy, V. v.; Dantus, M. Femtosecond Pulse Shaping Adds a New Dimension to Mass Spectrometry. *Appl. Opt.* **2007**, *46*, 4041−4045.
(37) Yan, L.; Cudry, F.; Li, W.; Suits, A. G. Isomer-Specific Mass Spectrometric Detection Via "Semisoft" Strong-Field Ionization. *J. Phys. Chem. A* **2013**, *117*, 11890−11895.
(38) Li, S.; Jochim, B.; Jackson, J. E.; Dantus, M. Femtosecond Dynamics and Coherence of Ionic Retro-Diels−Alder Reactions. *J. Chem. Phys.* **2021**, *155*, 044303.
(39) *Spartan*; Wavefunction Inc.: Irvine, 2018.
(40) Noutary, C. J. Mass Spectrometric Study of the Photoionization of Some Fluorocarbons and Trifluoromethyl Halides. *J. Res. Natl. Bur. Stand., A Phys. Chem.* **1968**, *72*, 479−485.
(41) Lifshitz, C.; Grajower, R. Dissociative Electron Capture and Dissociative Ionization in Perfluorocyclobutane. *Int. J. Mass Spectrom. Ion Phys.* **1972**, *10*, 25−37.

https://doi.org/10.1021/acs.jpca.2c05373
J. Phys. Chem. A 2022, 126, 8851−8858